J. Phys. B: At. Mol. Opt. Phys. **44** (2011) 165302 (7pp) doi:10.1088/0953-4075/44/16/165302

Spin domain wall in rotating two-component Bose–Einstein condensates

Jingjing Jin, Suying Zhang[1] and Wei Han

Institute of Theoretical Physics, Shanxi University, Taiyuan 030006, People's Republic of China

E-mail: zhangsy@sxu.edu.cn

Received 27 March 2011, in final form 19 May 2011
Published 20 July 2011
Online at stacks.iop.org/JPhysB/44/165302

Abstract

We study rotating two-component Bose–Einstein condensates with equal particle numbers and strong intercomponent repulsion located in a harmonic potential by numerically solving two-dimensional coupled Gross–Pitaevskii equations. The condensates are observed as a dramatic departure, forming a pair of shells located symmetrically in the trap with a small spatial overlap. Projecting the system into a pseudospin space, a spin domain wall is formed at the interface of the two components. The complex and spatial periodic spin texture is formed on the domain-wall region. We discuss the dependence of the spin texture of the domain wall on the angular velocity in detail. The relation among the number of the vortices, the topological charge and the angular momentum, as an extension of Feynman's rule in the two-component Bose–Einstein condensates, is given, based on the spin texture carrying the angular momentum of the condensates.

(Some figures in this article are in colour only in the electronic version)

1. Introduction

The study of Bose–Einstein condensation (BEC) in trapped atomic clouds opened up the exploration of quantum phenomena in a qualitatively new regime. Since BECs have been realized experimentally in a dilute bosonic gas [1, 2], many properties of these systems have been studied experimentally and theoretically [3]. The quantized vortex is the most famous topological defect in a single-component BEC, and the static and dynamic properties of vortices or vortex lattices have been investigated by a large number of theoretical and experimental workers [4–6]. Besides, the quantum turbulence has been extensively researched theoretically and numerically [7–9] and has been observed experimentally [10]. Recently, the new progress of two-component BECs gives us a possibility of constructing totally new topological objects in condensed matter physics. As the alkali atoms have hyperfine spin, two-component BECs can be considered two hyperfine-spin states located in the same trap [11, 12]. Many kinds of exotic topological defects such as coreless vortices [13] and skyrmions are excited because of the internal spin degrees of freedom [14] of the condensates, which are not accessible in a single-component condensate and have been studied recently in considerable detail in atomic BECs [15–21][2].

Two-component BECs have more interesting patterns of symmetry and symmetry breaking. The density patterns can be adjusted by changing the parameters of the system, such as the trapping frequencies, the relative particle numbers of two components or the atom–atom interactions. In particular, the intercomponent interaction determines whether the phases of the condensates are separated or not [22, 23]. Because the intra- and intercomponent scattering lengths are arbitrary by changing the s-wave scattering length via magnetic-field Feshbach resonances, a variety of miscibility or immiscibility of the two-component BECs have been observed experimentally [11, 24–26] and studied theoretically [22, 27–29].

In this paper, we first study the two-component BECs located in a harmonic trap with an equal number of particles ($N_1 = N_2$) and the same intracomponent s-wave scattering

[1] Author to whom any correspondence should be addressed.

[2] The observation of interlaced square vortex lattices in rotating spinor BECs has been reported recently in [18].

lengths ($a_{11} = a_{22}$). We choose the intercomponent s-wave scattering lengths larger than the intracomponent ones to satisfy [16, 22]

$$a_{12}^2 > a_{11}a_{22},$$

in order to make the two components spatially separate. Due to the strong intercomponent repulsion, we observe that the density distribution of the condensates shows a dramatic symmetrical departure in the trapping potential [30]. The two-component BECs can be represented in terms of the 'pseudospin' because of the spinor nature of the order parameters [14, 21, 31]. The pseudospin of one component points up and the other points down on both sides, correspondingly. At the interface of the two components, the pseudospin of the system twists and forms the spin domain wall. We study the dependence of spin texture of the domain wall on the angular velocity in detail. We give the relationship among the topological charge, the number of vortices and the angular momentum expectation, which is the generalized Feynman rule in the two-component Bose–Einstein condensates.

This paper is organized as follows. In section 2, we introduce the basic formulation of the problem. In section 3, the two-component condensates which have equal particle numbers and the same intracomponent scattering lengths, with an angular velocity in the isotropic trap, are produced numerically, and a spin domain wall with complex spin texture is obtained. In section 4, we discuss the properties of the condensates by changing the angular velocity and present the relationship among the topological charge, the number of the vortices and the angular momentum expectation. In section 5, the generalization about two condensates with unbalanced parameters is provided. The conclusions are given in section 6.

2. Formulation of the problem

The trapped two-component BECs are characterized by the condensate spatial wavefunctions $\psi = (\psi_1, \psi_2)^T$. In the weak interaction limit, the condensates in the frame rotating with angular velocity Ω around the z axis can be well described by the coupled Gross–Pitaevskii equations (CGPEs)

$$\mathrm{i}\hbar\frac{\partial\psi_j}{\partial t} = \left[-\frac{\hbar^2\nabla^2}{2m} + V + \sum_{k=1}^{2} g_{jk}\,|\psi_k|^2 - \Omega L_z\right]\psi_j, \qquad (1)$$

where ψ_j ($j = 1$ or 2) refers to the macroscopic wavefunction of the jth component. The parameters $g_{jk} = 4\pi\hbar^2 a_{jk}/m$ represent the intracomponent (g_{11}, g_{22}) and intercomponent (g_{12}, g_{21}) interactions characterized by the s-wave scattering length (a_{11}, a_{22}) between atoms in the same components and ($a_{12} = a_{21}$) between atoms in the different components. The wavefunctions are normalized as

$$\int (|\psi_1|^2 + |\psi_2|^2)\,\mathrm{d}\mathbf{r} = N_1 + N_2 = N,$$

where $N_1 = \int |\psi_1|^2\,\mathrm{d}\mathbf{r}$ and $N_2 = \int |\psi_2|^2\,\mathrm{d}\mathbf{r}$ are the particle numbers of the $j = 1$ and 2 components, respectively, and the total number of particles in the condensates is N. $L_z = -\mathrm{i}\hbar(x\partial y - y\partial x)$ is the z-component of the angular momentum operator. The trapping potential is assumed to be

$$V = \tfrac{1}{2}m\left(\omega_\perp^2(x^2 + y^2) + \omega_z^2 z^2\right).$$

For simplicity, we consider the situation that the condensate is tightly confined in the z axial direction $\left(\lambda = \frac{\omega_z}{\omega_\perp} \gg 1\right)$, i.e. it is a 'pancake-shaped' potential [32], so the two-dimensional (2D) approximation is implemented for the condensates.

In this paper, the scales of length, time, angular momentum and rotation angular velocity are chosen as $a_0 = \sqrt{\hbar/m\omega_\perp}$, $1/\omega_\perp$, $\hbar$ and $\omega_\perp$, respectively. Then we obtain the two-dimensional (2D) dimensionless coupled Gross–Pitaevskii equations

$$\mathrm{i}\frac{\partial\psi_j}{\partial t} = \left[-\frac{1}{2}\nabla^2 + V + \sum_{k=1}^{2}\beta_{jk}\,|\psi_k|^2 - \Omega L_z\right]\psi_j, \qquad (2)$$

where $V = \frac{1}{2}(x^2 + y^2)$, and the interaction coefficients are defined as

$$\beta_{jk} = 2\sqrt{2\pi\lambda}N_k a_{jk}/a_0.$$

3. Spin texture on the spin domain-wall region

We assume that the two condensates have an equal number of particles ($N_1 = N_2$), and we consider the case when the condensates have the same intracomponent s-wave scattering length ($a_{11} = a_{22}$). The intra- and intercomponent interactions of the system are chosen as $\beta_{11} = \beta_{22} = 50$, $\beta_{12} = 300$. A possible experimental case of ^{87}Rb which is condensed into two different hyperfine states can be considered. The condensates contain $N_1 = N_2 = 5 \times 10^4$ atoms, each of mass $m = 1.4188 \times 10^{-25}$ kg, and the scattering lengths are adjusted as $a_{11} = a_{22} = 16.5a$, $a_{12} = a_{21} = 99.0a$ by Feshbach resonances, where a is the Bohr radius. The trap with frequencies $\{\omega_\perp, \omega_z\} = 2\pi\,\{4.2, 38.6\}$ Hz. In this section, we consider the condensates with the rotation angular velocity $\Omega = 0.65\omega_\perp$ in the harmonic trap by solving equation (2). By using the imaginary time propagation method $t \to \tau = \mathrm{i}t$, the ground state is obtained. The density profile of the condensates is shown in figure 1. Due to the strong repulsive interaction between components, two condensates show dramatic departure and undergo phase separation with small spatial overlap, forming a pair of shells located symmetrically in the trap. $|1\rangle$ represents the condensate on the left and $|2\rangle$ represents that on the right. Figure 2 shows the effective velocity field of the two-component condensates, which is defined as

$$\upsilon_{\mathrm{eff}} = [j_1(r) + j_2(r)]/\rho_T(r), \qquad (3)$$

where $j_k = \frac{\hbar}{2\mathrm{i}m}\left(\psi_k^*\nabla\psi_k - \psi_k\nabla\psi_k^*\right)$ ($k = 1, 2$) is the partial current density [20] and $\rho_T(r)$ is the total density of the condensates. We can see that the two condensates have a total velocity around the trap centre without any vortices. This phenomenon reminds us that the condensates allow other topological excitations to carry angular momentum. We know that the spinor nature of two-component condensates can be described by the pseudospin-1/2-order parameters. We introduce a normalized complex-valued spinor $\chi = [\chi_1(\mathbf{r}), \chi_2(\mathbf{r})]^T = \left[|\chi_1|\,\mathrm{e}^{\mathrm{i}\theta_1}, |\chi_2|\,\mathrm{e}^{\mathrm{i}\theta_2}\right]^T$,

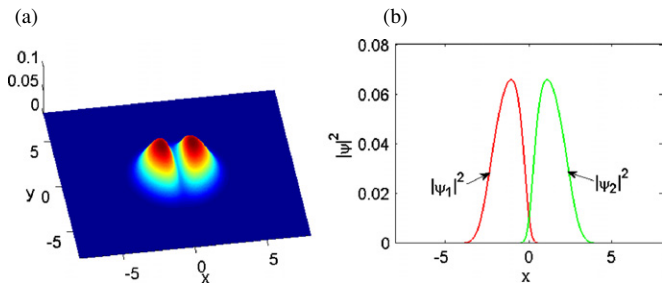

Figure 1. (a) The density profile of the two-component BECs consisting of the ψ_1 component on the left and the ψ_2 component on the right for $\beta_1 = \beta_2 = 50$, $\beta_{12} = 300$ and $\Omega = 0.65\omega_\perp$. (b) The cross sections of $|\psi_1|^2$ and $|\psi_2|^2$ along the x axis at $y = 0$.

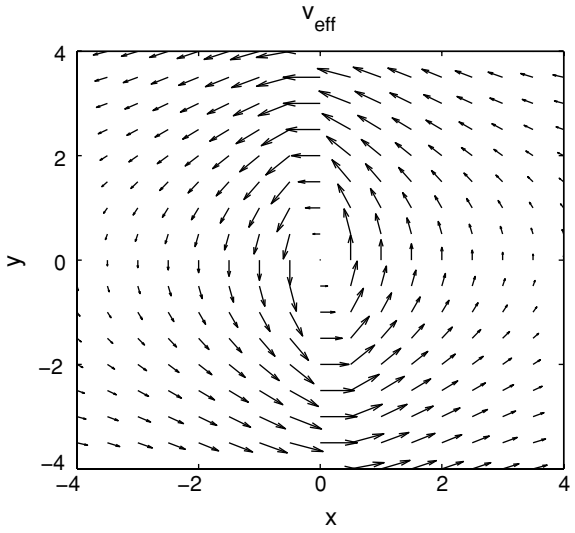

Figure 2. The vectorial plot of the effective velocity field v_{eff} of equation (3).

which satisfies $|\chi_1|^2 + |\chi_2|^2 = 1$, and θ_j are the phases of the condensate wavefunctions. Then the wavefunctions are decomposed as $\psi_j = \sqrt{\rho_T(\mathbf{r})}\chi_j(\mathbf{r})$. The pseudospin density is defined as $S = \bar{\chi}(\mathbf{r})\sigma\chi(\mathbf{r})$, where σ is the Pauli matrix. So the pseudospin density is expressed as

$$\begin{cases} S_x = 2\,|\chi_1|\,|\chi_2|\cos(\theta_1 - \theta_2), \\ S_y = -2\,|\chi_1|\,|\chi_2|\sin(\theta_1 - \theta_2), \\ S_z = |\chi_1|^2 - |\chi_2|^2\,, \end{cases} \tag{4}$$

and $|S| = \sqrt{S_x^2 + S_y^2 + S_z^2} = 1$.

We first consider the condensates without rotation, i.e. $\Omega = 0$. The pseudospin density distributions for S_z, S_x and S_y are shown in figures 3(a)–(c), respectively. The $|2\rangle$ component vanishes on the left and the spin points up; the $|1\rangle$ component vanishes on the right and the spin points down. The spin domains are formed. At the interface of the two condensates, the spin crosses the spin domain wall and twists through an angle of π from up to down continuously. It is notable that the spin on the domain-wall region aligns regularly with no projection onto the y-axis, i.e. the spin flips in the direction perpendicular to the domain wall, as shown in figures 3(c) and (d). We can understand this phenomenon from equation (4),

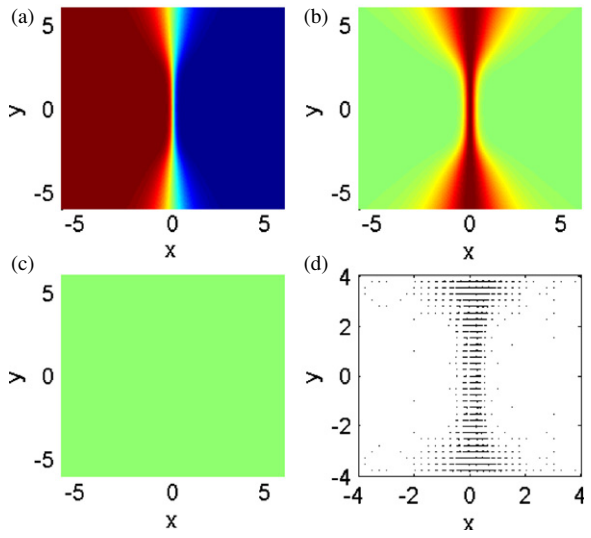

Figure 3. The pseudospin density $S = \bar{\chi}(\mathbf{r})\sigma\chi(\mathbf{r})$ distribution for (a) S_z, (b) S_x and (c) S_y for $\Omega = 0$. (d) The vectorial representation of the spin texture projected onto the x–y plane.

that is, when $\Omega = 0$, the two condensate phases satisfy $\theta_1 = \theta_2 = \text{constant}$, so $S_x = 2\,|\chi_1|\,|\chi_2|\cos(\theta_1 - \theta_2) = 2\,|\chi_1|\,|\chi_2|$ and $S_y = -2\,|\chi_1|\,|\chi_2|\sin(\theta_1 - \theta_2) = 0$.

When the condensates are under an angular velocity, e.g. $\Omega = 0.65\omega_\perp$, the spin on the domain wall has a complex twist. The spin twists not only in the direction perpendicular to the domain wall, but also in the direction parallel to the domain wall, as shown in figure 4. This spin twist gives rise to a complex and spatial periodic spin texture, and it can be understood that the rotating two-component condensates tend to carry angular momentum by exciting this new topological structure. Moreover, because two components have a relative motion at the interface, the possible mechanism of this spin texture excitation is Kelvin–Helmholtz instabilities [10, 33]. Furthermore, from figures 4(b) and (c), we can see that the chain-like pseudospin density distribution for S_x is even parity and for S_y is odd parity. The projected vectorial plot of (S_x, S_y) is shown in figure 5. It is notable that we study this spin texture in the case of two-dimensional approximation; in fact, the topological structure is nearly not affected by the third dimension. But the thickness of the domain wall on the different cross sections which are parallel to the x–y plane will be varied because of the impact of the three-dimensional trapping potential.

It is well known that the topological charge density is defined as

$$q(\mathbf{r}) = \frac{1}{8\pi}\epsilon^{ij}\mathbf{S}\cdot\partial_i\mathbf{S}\times\partial_j\mathbf{S}. \tag{5}$$

As shown in figure 4(d), the topological charge density concentrated on the domain-wall region is elongated. $Q = \int \mathrm{d}\mathbf{r}q(\mathbf{r})$ is called a topological charge or the Pontryagian index [34]. After numerical calculation, we find that the topological charge is fractional in our situation. It is different from those of previous papers which show that the topological charge is an integer [19, 20]. We discuss the reason why Q is fractional in our situation in the following section.

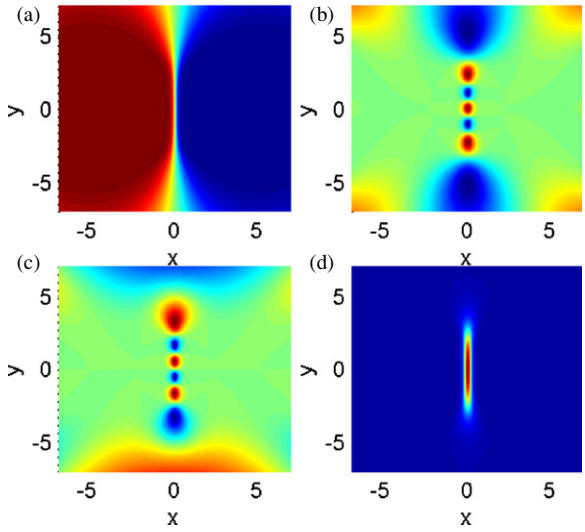

Figure 4. The pseudospin density $S = \bar{\chi}(\mathbf{r})\sigma\chi(\mathbf{r})$ distribution for (a) S_z, (b) S_x and (c) S_y for $\Omega = 0.65\omega_\perp$. (d) The distribution of the topological charge density $q(\mathbf{r})$ of equation (5).

4. Dependence

In this section, we research the properties of the condensates with different Ω. Figure 6 shows the density and pseudospin density of the condensates with different Ω. As Ω increases, the particle distribution of condensates expands away from the trap centre due to the centrifugal effect. The space occupancy of the condensates expands along the direction which is parallel to the direction of the domain wall, but keeps approximately constant along the direction which is perpendicular to the direction of the domain wall until $\Omega = \Omega_c = 0.78\omega_\perp$, as shown in figures 6(a) and 7. When $\Omega = \Omega_c$, a pair of vortices appear in the condensates, and the vortex lattices appear in the condensates when Ω increases further. The space occupancy of the condensates expands not only along the direction parallel to the domain wall, but also along the direction perpendicular to the domain wall when $\Omega \geqslant \Omega_c$. With increasing Ω, a longer periodic

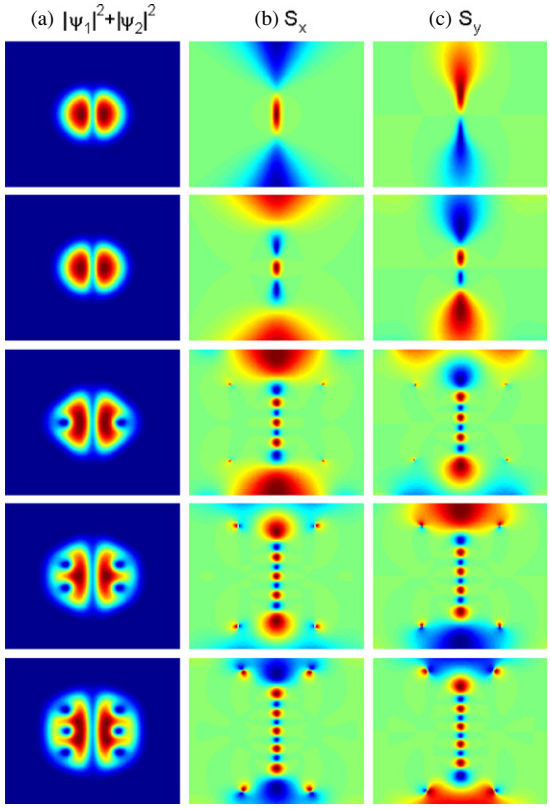

Figure 6. (a) The total density distributions ρ_T of the condensates for different rotating velocities: $\Omega = 0.2\omega_\perp$, $\Omega = 0.4\omega_\perp$, $\Omega = 0.78\omega_\perp$, $\Omega = 0.85\omega_\perp$, $\Omega = 0.9\omega_\perp$, respectively. (b) The pseudospin density distributions for (b)S_x and (c) S_y corresponding to (a).

spin texture with bigger topological charge is formed in order to carry more angular momentum, as shown in figures 6(b) and (c). The chain-like density distribution of S_x and S_y at both ends of the domain wall increases and squeezes into the interface of the two condensates gradually. It is notable that the complete periodic structure corresponds to the integral topological charge; moreover, the periodic and the topological charges are of the same value, but the incomplete structure

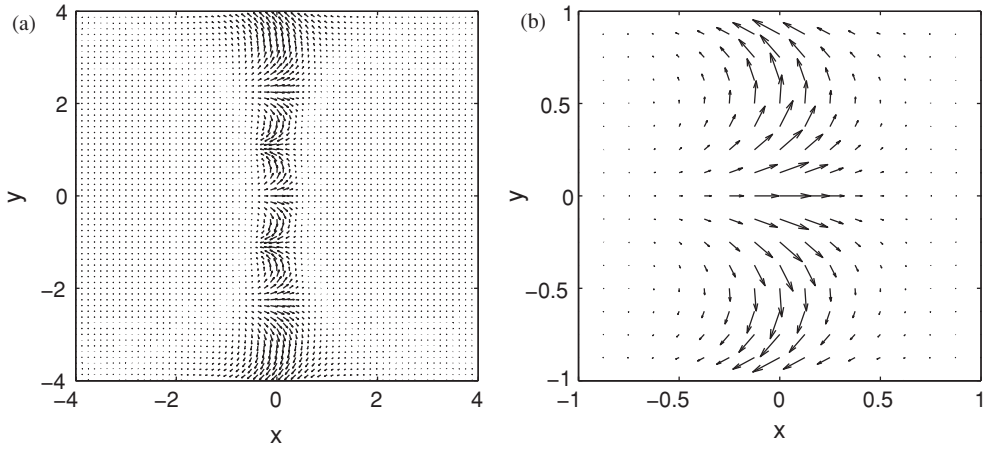

Figure 5. (a) The vectorial representation of the spin texture projected onto the x–y plane in the region $[-4 \leqslant x, y \leqslant +4]$ for $\Omega = 0.65\omega_\perp$. (b) An amplification of the local part of (a).

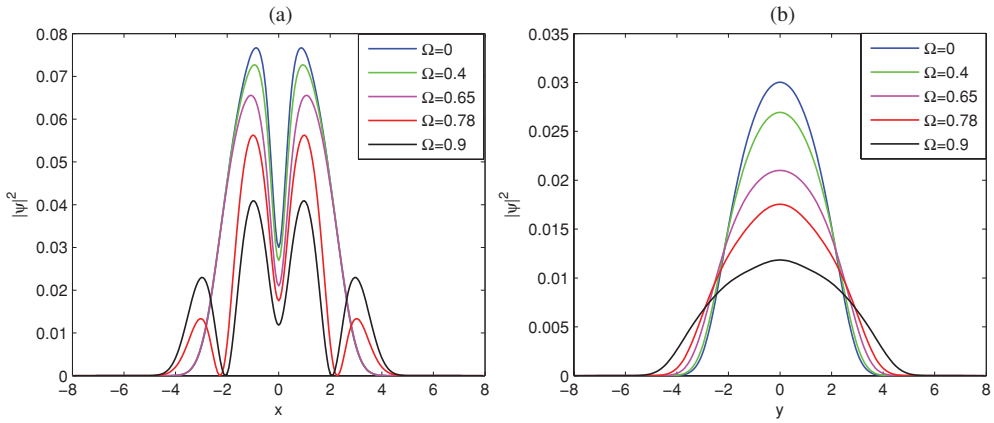

Figure 7. (a) The cross sections of the total density ρ_T along the x axis at $y = 0$. (b) The cross sections of the total density ρ_T along the y axis at $x = 0$.

at both ends of the domain wall corresponds to the fractional topological charge.

The dependence of the topological charge Q on the rotating frequency Ω is shown in figure 8(a). We can see that the topological charge increases gradually and continuously with Ω until a drop occurs at $\Omega_c = 0.78\omega_\perp$. When $\Omega = \Omega_c$, a pair of vortices appear in the condensates as shown in figure 6(a). At the same time, the vortices share the angular momentum with the spin texture on the domain-wall region, so the topological charge decreases abruptly. In addition, we also find that, for $\Omega < \Omega_c$, Q increases linearly, and for $\Omega \geqslant \Omega_c$, Q increases exponentially. It can be interpreted that the condensates expand slowly along the direction of the domain wall as Ω increases, but expand rapidly when the vortices appear.

Figure 8(b) shows the dependence of the sum of the topological charge Q and the number of vortices N_v on the angular velocity $\Omega/\omega_\perp$, and the angular momentum expectation per atom,

$$\langle L_z/\hbar\rangle = \sum_j \int \psi_j^*(\mathbf{r})\,(L_z/\hbar)\,\psi_j(\mathbf{r})\,\mathrm{d}\mathbf{r}. \tag{6}$$

Comparing figure 8(b) with figure 8(a), we can find that $\Omega = 0.78\omega_\perp$ is still a breakpoint. The difference between the two figures at this point is that the value of $\langle L_z/\hbar\rangle$ makes a jump but the topological charge Q makes a drop. The angular momentum expectation increases linearly for $\Omega < \Omega_c$ and increases exponentially for $\Omega \geqslant \Omega_c$. It may be associated with the fact that when $\Omega < \Omega_c$, the angular momentum is carried only by the spin texture, and the spin texture is only formed on the domain-wall region. But when $\Omega \geqslant \Omega_c$, the angular momentum is carried not only by the spin texture but also by the vortices, and the vortices are formed in the whole region of the condensates.

From figure 8, we find that the topological charge, the number of the vortices and the angular momentum expectation satisfy the relation

$$\langle L_z/\hbar\rangle = \frac{Q + N_v}{2}, \tag{7}$$

where N_v is the total number of the vortices in the condensates. For the case of $\Omega < \Omega_c$, there is no vortices in the condensates,

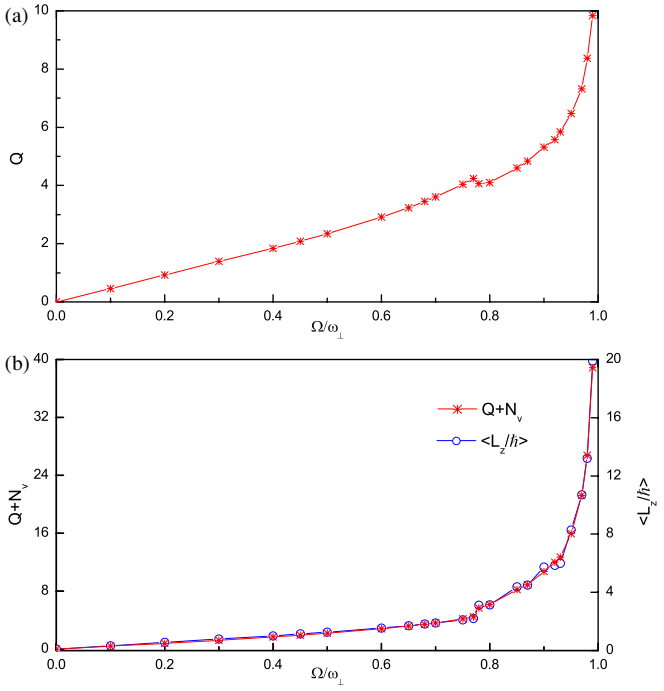

Figure 8. (a) The topological charge for several values of the rotation velocity Ω. (b) The sum of the topological charge and the number of the vortices for several values of the rotation velocity Ω , and the angular momentum per atom for different Ω.

i.e. $N_v = 0$, so $\langle L_z/\hbar\rangle = \frac{Q}{2}$. This is understood by the simple model in which the rotating condensate with a spin domain wall is considered as a rigid-body rotation. Although the two components depart from each other in the trap, the total density profile has the same shape with the trap. Then the mean angular momentum per atom at $r = \sqrt{x^2 + y^2}$ is $L_z/\hbar = m\Omega r^2/\hbar$, where m is the mass of the atom. The average of the angular momentum per atom averaged over the whole condensates is given by

$$\langle L_z/\hbar\rangle = \frac{\sum_j \int \psi_j^*\,(L_z/\hbar)\,\psi_j\,\mathrm{d}\mathbf{r}}{\sum_j \int |\psi_j|^2\,\mathrm{d}\mathbf{r}}. \tag{8}$$

Assuming the spatially homogeneous total density, we obtain

$$\langle L_z/\hbar\rangle = \frac{m\Omega R^2}{2\hbar}, \tag{9}$$

with the typical radius R of the condensates. The topological charge density and the effective velocity satisfy the relationship [19, 35]

$$q(\mathbf{r}) = \frac{1}{8\pi}\epsilon^{ij}\mathbf{S}\cdot\partial_i\mathbf{S}\times\partial_j\mathbf{S} = \frac{m}{2\pi\hbar}(\nabla\times\upsilon_{\rm eff})_z\,. \tag{10}$$

So the topological charge can be obtained by an integral,

$$Q = \int \frac{m}{2\pi\hbar}(\nabla\times\upsilon_{\rm eff})_z\,\mathrm{d}\mathbf{r}$$
$$= \frac{m}{2\pi\hbar}\int(\nabla\times\Omega\times\mathbf{r})\,\mathrm{d}\mathbf{r},$$

yielding

$$Q = \frac{m\Omega R^2}{\hbar}. \tag{11}$$

We obtain

$$\langle L_z/\hbar\rangle = \frac{Q}{2}. \tag{12}$$

For the case of $\Omega \geqslant \Omega_c$, the angular momentum is carried by both the spin domain wall and the vortices, so

$$\int(\nabla\times\upsilon_{\rm eff})_z\,\mathrm{d}\mathbf{r} = \frac{\hbar}{m}2\pi\,(Q+N_v)\,, \tag{13}$$

where we used Feynman's rule $\oint_l \upsilon\cdot\mathrm{d}\mathbf{l} = \frac{\hbar}{m}2\pi N_v$ which is obtained from a single-component BEC. Similarly, approximating equation (13) with rigid-body rotation, we obtain equation (7). As we know, in a single-component BEC, assuming the spatially homogeneous density, the condensate with a dense vortex lattice should be regarded as a rigid-body rotation [36], Feynman's rule can be expressed as $\left\langle\frac{L_z}{\hbar}\right\rangle = \frac{N_v}{2}$ [32], which gives the relationship of the total number of vortices and the angular momentum. In our case, the spin texture also carries angular momentum like the vortices. Therefore, with the topological charge included, Feynman's rule is extended to the form of equation (7) in the two-component BECs, and is in good agreement with the numerical results. Furthermore, due to the topological charge which in our case is fractional, as long as the angular velocity is not equal to 0, there is a non-zero angular momentum and non-zero topological charge even if the angular velocity is small. It is different from the case of the single-component BEC that there is a non-zero angular momentum only if the angular velocity exceeds the critical value.

5. Generalization

In this paper, we mainly study two condensates that have an equal number of particles and the same intracomponent s-wave scattering length. For generalized cases, if two components have an equal number of particles, but slightly different intracomponent s-wave scattering lengths, e.g. $N_1 = N_2 = 5\times10^4$, $a_{11} = 16.5a$, $a_{22} = 26.4a$; or the same intracomponent s-wave scattering length, but a small imbalance particle number, e.g. $N_1 = 4.9\times10^4$, $N_2 = 5.1\times10^4$, $a_{11} = a_{22} = 16.5a$, the intracomponent mean-field interaction coefficients (β_{11}, β_{22}) are unequal, and the intercomponent interaction coefficients (β_{21}, β_{12}) may be unequal. Without loss of generality, we discuss the case when condensates have equal particle numbers but different intracomponent scattering lengths. The symmetry of the density distribution of two components is broken, so the interface of two components becomes curved, as shown in figure 9(a), and the component with strong interaction curves towards the one with weak interaction. The pseudospin density distributions for S_x and S_y are shown in figures 9(b) and (c). At the spin domain-wall region, the similar topological structure is formed. The distribution of the topological charge density is curved rather than straight, just like a crescent moon, as shown in figure 9(d), which is different from the case discussed in section 3. Increasing the rotating frequency, a more curved spin texture with more topological charge appears. Besides, if two components are respectively located in slightly different traps which are isotropic and have the same symmetry axis, a curved spin texture also appears, and the component which is tightly trapped will curve towards the loose one. We find that, for the two condensates, with slight inequality in intracomponent interactions or small imbalance in particle number, or located in slightly different traps, the similar topological spin texture is excited, and equation (7) is still valid. When the above-mentioned parameters are quite different, different topological structure will appear, e.g. the big skyrmion [20]. Due to the emergence of a giant vortex, equation (7) is invalid.

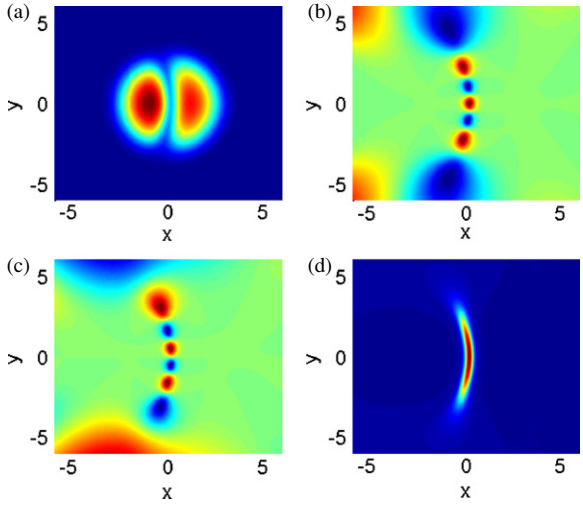

Figure 9. (a) The density profile of the two-component BECs for $\beta_{11} = 50$, $\beta_{22} = 60$, $\beta_{12} = \beta_{21} = 300$ and $\Omega = 0.65\omega_\perp$. The corresponding pseudospin density distribution for (b) S_x and (c) S_y. (d) The distribution of the topological charge density $q(\mathbf{r})$.

6. Conclusion

In conclusion, we have discussed the two-component condensates with the strong intercomponent repulsion and their corresponding pseudospin textures in a rotating harmonic potential. At the interface of the two components, the non-zero pseudospin projection on the x–y plane shows that the

pseudospin twists from up to down through an angle of π. A complex and spatial periodic spin texture is formed on the domain-wall region. As the angular velocity increases, in order to carry more angular momentum, the spin texture with more periods becomes longer gradually and the topological charge becomes bigger correspondingly. Both of the topological charge and the angular momentum expectation per atom increase linearly until the angular velocity exceeds the critical value, and then increase exponentially. Considering the angular momentum shared by the spin texture and the vortices, we extend Feynman's rule to the two-component condensates with the topological charge included.

Acknowledgments

This work was supported by National Natural Science Foundation of China (10972125), Natural Science Foundation of Shanxi Province (2010011001-2) and Special Foundation for Returnee of Shanxi Province.

References

[1] Anderson M H, Ensher J R, Matthewa M R, Wieman C E and Cornell E A 1995 Observation of Bose–Einstein condensation in a dilute atomic vapor *Science* **269** 198–201
[2] Bradley C C, Sackett C A, Tollett J J and Hulet R G 1995 Evidence of Bose–Einstein condensation in an atomic gas with attractive interaction *Phys. Rev. Lett.* **75** 1687–90
[3] Dalfovo F, Giorgini S, Pitaevskii L and Stringari S 1999 *Rev. Mod. Phys.* **71** 463
[4] Abo-Shaeer J R *et al* 2001 *Science* **292** 476
[5] Raman C, Abo-Shaeer J R, Vogels J M, Xu K and Ketterle W 2001 *Phys. Rev. Lett.* **87** 210402
[6] Fetter A L 2009 *Rev. Mod. Phys.* **81** 647
[7] Kobayashi M and Tsubota M 2007 *Phys. Rev.* A **76** 045603
[8] Parker N G and Adams C S 2005 *Phys. Rev. Lett.* **95** 145301
[9] Weiler C N *et al* 2008 *Nature* **455** 948
[10] Henn E A L, Seman J A, Roati G, Magalhaes K M F and Bagnato V S 2009 *Phys. Rev. Lett.* **103** 045301
[11] Hall D S, Matthews M R, Ensher J R, Wieman C E and Cornell E A 1998 *Phys. Rev. Lett.* **81** 1539
[12] Stenger J, Inouye S, Stamper-Kurn D M, Miesner H-J, Chikkatur A P and Ketterle W 1998 *Nature* **369** 345
[13] Leanhardt A E, Shin Y, Kielpinski D, Pritchard D E and Ketterle W 2003 *Phys. Rev. Lett.* **90** 140403
[14] Pethik C J and Smith H 2002 *Bose–Einstein Condensation in Dilute Gases* (Cambridge: Cambridge University Press)
[15] For a brief review, see Girvin S M 2000 *Phys. Today* **53** 39 (and references therein)
[16] Battye R A *et al* 2002 *Phys. Rev. Lett.* **88** 80401
[17] Savage C M and Ruostekoski J 2003 *Phys. Rev. Lett.* **91** 010403
[18] Schweikhard V, Coddington I, Engels P, Tung S and Cornell E A 2004 *Phys. Rev. Lett.* **93** 210403
[19] Kasamatsu K, Tsubota M and Ueda M 2005 *Phys. Rev.* A **71** 043611
[20] Yang S-J, Wu Q-S, Zhang S-N and Feng S 2008 *Phys. Rev.* A **77** 033621
[21] Leslie L S, Hansen A, Wright K C, Deutsch B M and Bigelow N P 2009 *Phys. Rev. Lett.* **103** 250401
[22] Ho T-L and Shenoy V B 1996 *Phys. Rev. Lett.* **77** 3276
[23] Timmermans E 1998 *Phys. Rev. Lett.* **81** 5718
[24] Modugno G, Modugno M, Riboli F, Roati G and Inguscio M 2002 *Phys. Rev. Lett.* **89** 190404
[25] Thalhammer G, Barontini G, De Sarlo L, Catani J, Minardi F and Inguscio M 2008 *Phys. Rev. Lett.* **100** 210402
[26] Papp S B, Pino J M and Wieman C E 2008 *Phys. Rev. Lett.* **101** 040402
[27] Ao P and Chui S T 1998 *Phys. Rev.* A **58** 4836
[28] Trippenbach M, Góral K, Rzazewski K, Malomed B and Band Y B 2000 *J. Phys. B: At. Mol. Opt. Phys.* **33** 4017
[29] Kasamatsu K and Tsubota M 2004 *Phys. Rev. Lett.* **93** 100402
Kasamatsu K and Tsubota M 2006 *Phys. Rev.* A **74** 013617
[30] Esry B D, Greene C H, Burke J P Jr and Bohn J L 1997 *Phys. Rev. Lett.* **78** 3594
[31] Matthews M R, Anderson B P, Haljan P C, Hall D S, Wieman C E and Cornell E A 1999 *Phys. Rev. Lett.* **83** 2498
[32] Kasamatsu K, Tsubota M and Ueda M 2003 *Phys. Rev.* A **67** 033610
[33] Volovik G E 2002 *JETP Lett.* **75** 418
[34] Son D T and Stephanov M A 2002 *Phys. Rev.* A **65** 063621
[35] Mueller E J 2004 *Phys. Rev.* A **69** 033606
[36] Feder D L and Clark C W 2001 *Phys. Rev. Lett.* **87** 190401